3752 *Inorg. Chem.* **2010**, *49*, 3752–3763
DOI: 10.1021/ic902100v

Inorganic Chemistry
Article

A Triphenylamine-Grafted Imidazo[4,5-*f*][1,10]phenanthroline Ruthenium(II) Complex: Acid−Base and Photoelectric Properties

Su-Hua Fan,[†] An-Guo Zhang,[†] Chuan-Chuan Ju,[†] Li-Hua Gao,[‡] and Ke-Zhi Wang*,[†]

[†]*College of Chemistry, Beijing Normal University, Beijing 100875, People's Republic of China , and* [‡]*College of Chemistry and Environmental Engineering, Beijing Technology and Business University, Beijing 100037, People's Republic of China*

Received October 23, 2009

A new heteroleptic ruthenium(II) complex of $[Ru(Hipdpa)(Hdcbpy)(NCS)_2]^- \cdot 0.5H^+ \cdot 0.5[N(C_4H_9)_4]^+$ **Ru**(**Hipdpa**) {where Hdcbpy = monodeprotonated 4,4′-dicarboxy-2,2′-bipyridine and Hipdpa = 4-(1*H*-imidazo[4,5-*f*][1,10]phenanthrolin-2-yl)-*N*,*N*-diphenylaniline} was synthesized and characterized by elementary analysis, standard spectroscopy techniques, and cyclic voltammetry. The ground- and excited-state acid−base properties of **Ru**(**Hipdpa**) were studied by means of UV−vis absorption spectrophotometric and spectrofluorimetric titrations in 4:1(v/v) Britton-Robinson/dimethylformamide buffer solution. The four-step separate protonation/deprotonation processes were found in the ground states, and one of which taking place near the physiological pH range. The two observable excited-state protonation/deprotonation processes were found for the **Ru**(**Hipdpa**), constituting pH-induced "off−on−off" emission switches. The performance of the complexes as photosensitizers in nanocrystalline TiO_2-based liquid solar cells containing an electrolyte solution (0.05 M I_2, 0.5 M LiI, and 0.5 M 4-*tert*-butylpyridine in 50% acetonitrile and 50% propylene carbonate) was investigated and found to achieve a much improved device performance (a short-circuit photocurrent density of 18.7 mA cm^{-2}, an open-circuit voltage of 630 mV, and an overall conversion efficiency of 6.85%) compared to a triphenylamine-free parent complex $[Ru(Hpip)(Hdcbpy)(NCS)_2]^- \cdot [N(C_4H_9)_4]^+$-based device {Hpip = 2-phenyl-1*H*-imidazo[4,5-*f*][1,10]phenanthroline} and a comparable performance to that of *cis*-bis(isothiocyanato)bis(2,2′-bipyridine-4,4′-dicarboxylic acid)ruthenium(II) (**N3**) under identical experimental conditions. A density functional theory calculation of the molecular structures and electronic properties of the complexes was also carried out in an effort to understand their effectiveness in TiO_2-based solar cells.

Introduction

Dye-sensitized solar cells (DSSCs) have attracted greater attention in industry and academic research because of their great potential to convert solar energy into electrical energy efficiently at low cost.[1] Generally, the DSSCs consist of photosensitizers adsorbed on a mesoporous nanocrystalline semiconductor thin film electrode, electrolyte, and counter electrode. The photosensitizers, which has a capacity of interacting with sunlight and can promote the photoinduced electron transfer to the conduction band of TiO_2 semiconductor and of transferring hole to redox species, play a crucial role in getting a higher solar-to-electricity conversion efficiency and have been a subject of active investigations.[2] The polypyridyl ruthenium(II) complex-based dyes have been evidenced to be one family of the most widely studied efficient charge-transfer photosensitizers, owing to their broad and strongly absorbing metal-to-ligand charge-transfer (MLCT) absorption bands, chemical stability of photoexcited states, and oxidized form.[3] The paradigms include *cis*-$Ru(H_2dcbpy)_2(NCS)_2$ (H_2dcbpy = 2,2′-bipyridyl-4,4′-dicarboxylic acid), which is referred to as **N3**,[4,5] and tris(isothiocyanato)-2,2′,2″-terpyridyl-4,4′,4″-tricarbolylate)ruthenium(II) complex, which is referred to as black dye, have visible absorption extending into the near-IR region up to 920 nm, producing an overall efficiency of 10.4%.[6] In recent years, many groups have reported a very popular family of heteroleptic ruthenium complexes of the type $Ru(H_2dcbpy)(L')(NCS)_2$ by changing

*Corresponding author. Telephone: +86-10-58805467. Fax: +86-10-58802075. E-mail: kzwang@bnu.edu.cn.

(1) (a) O'Regan, B.; Grätzel, M. *Nature* **1991**, *353*, 737. (b) Grätzel, M. *Inorg. Chem.* **2005**, *44*, 6841. (c) Hagfeldt, A.; Grätzel, M. *Acc. Chem. Res.* **2000**, *33*, 269.

(2) (a) Park, N. G.; van de Lagemaat, J.; Frank, A. J. *J. Phys. Chem. B* **2000**, *104*, 8989. (b) Hauch, A.; Georg, A. *Electrochim. Acta* **2001**, *46*, 3457. (c) Kumar, R.; Sharma, A. K.; Parmar, V. S.; Watterson, A. C.; Chittibabu, K. G.; Kumar, J.; Samuelson, L. A. *Chem. Mater.* **2004**, *16*, 4841. (d) Robertson, N. *Angew. Chem., Int. Ed.* **2006**, *45*, 2338. (e) Durrant, J. R.; Haque, S. A.; Palomares, E. *Chem. Commun.* **2006**, 3279. (f) Qi, Z. M.; Wei, M. D.; Honma, I.; Zhou, H. *ChemPhysChem* **2007**, *8*, 264.

(3) (a) Hoertz, P. G.; Mallouk, T. E. *Inorg. Chem.* **2005**, *44*, 6828. (b) Meyer, G. J. *Inorg. Chem.* **2005**, *44*, 6852.

(4) Nazeeruddin, M. K.; Humphry-Baker, R.; Liska, P.; Grätzel, M. *J. Phys. Chem. B* **2003**, *107*, 8981.

(5) Hou, Y. J.; Xie, P. H.; Jing, Z.; Zhang, B. W.; Cao, Y.; Xiao, X. R.; Wang, W. B. *Inorg. Chem.* **1999**, *38*, 6320.

 Published on Web 03/25/2010

the ancillary ligand L′.[7] The carboxyl groups on H_2dcbpy in the complexes are responsible for the dye adsorption onto the semiconductor surface. The ancillary ligand L′ is not directly attached onto the semiconductor but can be used for tuning the overall properties of the complexes.

Triphenylamine (TPA) and related moieties have been widely employed as active components in optoelectric devices, such as light emitting[8] and photovolatic devices,[9,10] because of their desirable electron-donating and hole-transport capabilities.[11] Theoretical and experimental studies have also demonstrated that the TPA unit can also suppresses the dye aggregation due to its nonplanar structure. The incorporation of hole-conductors of TPA and phenothiazine moieties into Ru(II) complexes to synthesize supersensitizers have been proved to exhibit supersensitized effects by retarding interfacial charge-recombination dynamics and thus achieving long-lived photoinduced charge separation,[7a] which is a crucial strategy to enhance the performance of solar cells.[12] This kind of "donor-antenna" type ruthenium supersensitizers have also been successfully applied in solid-state DSSCs by Thelakkat et al.,[12b−d] obtaining the better device performance compared to the standard di(tetrabutylammonium) *cis*-bis(isothiocyanato)bis(2,2′-bipyridine-4-carboxylic acid-4′-carboxylate)ruthenium(II) (**N719**)-based cell.[13] Very recently, Wu and Ho et al.[12h] have applied two thiophenecarbazole-containing supersensitizers for liquid-state DSSCs, giving the device performance comparable to **N3**-based devices. These supersensitizers in liquid solar cells did not exhibit much improved device performance compared to their parent dye **N3**-based devices due probably to their large molecular sizes, in spite of the fact that their molar absorptivities are enhanced compared to **N3**.[12e,h] Also, among the Ru(II) complex-based photosensitizers developed for dye-sensitized solar cells, the incorporation of 1,10-phenanthroline derivative-containing ligands has received a little attention.[14]

On the other hand, the imidazole-containing ligands are poor π acceptors and good π donors and also have the ability to control orbital energies, so electron- and energy-transfer processes by proton transfer may produce interesting proton-induced on−off emission switches for the complexes, where the imidazole rings are coordinated or uncoordinated to the central metal ions.[15] Therefore, the imidazole group was also used to tune the ground- and excited-state properties of the Ru(II) complex in this work.

In continuation of our project on incorporation of carbazole and TPA moieties into electroluminescent materials,[16a−c] pH-induced luminescence switches, DNA intercalatively binding regents,[16d,e] and solar cell sensitizers,[14c] we have designed and synthesized a TPA-grafted ruthenium complex $[Ru(Hipdpa)(Hdcbpy)(NCS)_2]^- \cdot 0.5H^+ \cdot 0.5[N(C_4H_9)_4]^+$ **Ru(Hipdpa)** {where Hdcbpy = monodeprotonted-4,4′-dicarboxy-2,2′-bipyridine and Hipdpa = 4-(1*H*-imidazo[4,5-*f*]-[1,10]phenanthrolin-2-yl)-*N*,*N*-diphenylaniline}. Here, we report the acid−base and photoelectric properties of **Ru(Hipdpa)** as well as density functional theory (DFT) insights into the optimized geometries and electronic structures and the localizations of the frontier orbitals of the dyes.

Experimental Section

Synthesis of $[Ru(Hipdpa)(Hdcbpy)(NCS)_2]^- \cdot 0.5H^+ \cdot 0.5[N(C_4H_9)_4]^+ \cdot DMF \cdot 2H_2O$. Dichloro(*p*-cymene)ruthenium(II) dimer $[RuCl_2(p\text{-cymene})]_2$ (122 mg, 0.2 mmol) was dissolved in 30 mL of freshly distilled *N*,*N*-dimethylformamide (DMF), and Hipdpa (185.2 mg, 0.4 mmol) was added under a N_2 atmosphere. The reaction mixture was heated at 80 °C for 4 h under nitrogen, the H_2dcbpy (97.6 mg, 0.4 mmol) was added, and the reaction mixture was refluxed at 160 °C for an additional 4 h under dark. Then 20-fold excess of NH_4NCS (456 mg, 6 mmol) was added to the reaction mixture and heated at 130 °C for a further 5 h. The mixture was cooled to room temperature and was vacuum filtered. The filtrate was concentrated to ∼5 mL by rotary evaporation, water was then added to the resulting slurry, and the insoluble product was collected and washed with distilled water, followed by diethyl ether, affording a purple-black solid. The crude product was dissolved in DMF and allowed to crystallize by slow diffusion of diethyl ether before charging on

(6) Nazeeruddin, M. K.; Péchy, P.; Renouard, T.; Zakeeruddin, S. M.; Humphry-Baker, R.; Comte, P.; Liska, P.; Cevey, L.; Costa, E.; Shklover, V.; Spiccia, L.; Deacon, G. B.; Bignozzi, C. A.; Grätzel, M. *J. Am. Chem. Soc*. **2001**, *123*, 1613.

(7) (a) Hirata, N.; Lagref, J. J.; Palomares, E. J.; Durrant, J. R.; Nazeeruddin, M. K.; Grätzel, M.; Di Censo, D. *Chem.—Eur. J*. **2004**, *10*, 595. (b) Hara, K.; Horiuchi, H.; Katoh, R.; Singh, L. P.; Sugihara, H.; Sayama, K.; Murata, S.; Tachiya, M.; Arakawa, H. *J. Phys. Chem. B* **2002**, *106*, 374. (c) Hsu, Y. C. H.; Zheng, G.; Lin, J. T.; Ho, K. C. *Sol. Energy Mater. Sol. Cells* **2005**, *87*, 357. (d) Nazeeruddin, Md. K.; Klein, C.; Liska, P.; Grätzel, M. *Coord. Chem. Rev*. **2005**, *249*, 1460.

(8) Mitschke, U.; Bäuerle, P. *J. Mater. Chem*. **2000**, *10*, 1471.

(9) (a) Gunes, S.; Neugebauer, H.; Sariciftci, N. S. *Chem. Rev*. **2007**, *107*, 1324. (b) Kitamura, T.; Ikeda, M.; Shigaki, K.; Inoue, T.; Anderson, N. A.; Ai, X.; Lian, T. Q.; Yanagida, S. *Chem. Mater*. **2004**, *16*, 1806. (c) Hagberg, D. P.; Edvinsson, T.; Marinado, T.; Boschloo, G.; Hagfeldt, A.; Sun, L. C. *Chem. Commun*. **2006**, 2245.

(10) (a) Velusamy, M.; Thomas, K. R. J.; Lin, J. T.; Hsu, Y. C.; Ho, K. C. *Org. Lett*. **2005**, *7*, 1899. (b) Liang, M.; Xu, W.; Cai, F. S.; Chen, P.; Peng, B.; Chen, J.; Li, Z. M. *J. Phys. Chem. C* **2007**, *111*, 4465.

(11) (a) Lee, S. K.; Ahn, T.; Cho, N. S.; Lee, J. I.; Jung, Y. K.; Lee, J.; Shim, H. K *J. Polym. Sci., Part A-1: Polym. Chem*. **2007**, *45*, 1199. (b) Choi, H.; Baik, C.; Kang, S. O.; Ko, J.; Kang, M. S.; Nazeeruddin, Md. K.; Grätzel, M. *Angew. Chem., Int. Ed*. **2008**, *120*, 333.

(12) (a) Argazzi, R.; Bignozzi, C. A.; Heimer, T. A.; Castellano, F. N.; Meyer, G. J. *J. Am. Chem. Soc*. **1995**, *117*, 11815. (b) Karthikeyan, C. S.; Wietasch, H.; Thelakkat, M. *Adv. Mater*. **2007**, *19*, 1091. (c) Haque, S. A.; Handa, S.; Peter, K.; Palomares, E.; Thelakkat, M.; Durrant, J. R. *Angew. Chem., Int. Ed*. **2005**, *44*, 5740. (d) Karthikeyan, C. S.; Thelakkat, M. *Inorg. Chim. Acta* **2008**, *361*, 635. (e) Moser, J. E. *Nat. Mater*. **2005**, *4*, 723. (f) Jin, Z. Z.; Masuda, H.; Yamanaka, N.; Minami, M.; Nakamura, T.; Nishikitani, Y. *ChemSusChem* **2008**, *1*, 901. (g) Bonhote, P.; Moser, J. E.; Humphry-Baker, R.; Vlachopoulos, N.; Zakeeruddin, S. M.; Walder, L.; Gratzel, M. *J. Am. Chem. Soc*. **1999**, *121*, 1324. (h) Chen, C. Y.; Chen, J. G.; Wu, S. J.; Li, J. Y.; Wu, C. G.; Ho, K. C. *Angew. Chem., Int. Ed*. **2008**, *120*, 7452. (i) Qin, P.; Linder, M.; Brinck, T.; Boschloo, G.; Hagfeldt, A.; Sun, L. C. *Adv. Mater*. **2009**, *21*, 1.

(13) (a) Bach, U.; Lupo, D.; Comte, P.; Moser, J. E.; Weissortel, F.; Salbeck, J.; Spreitzer, H.; Gratzel, M. *Nature* **1998**, *395*, 583. (b) Nazeeruddin, M. K.; Kay, A.; Rodicio, I.; Humphrybaker, R.; Muller, E.; Liska, P.; Vlachopoulos, N.; Gratzel, M. *J. Am. Chem. Soc*. **1993**, *115*, 6382.

(14) (a) Onozawa-Komatsuzaki, N.; Kitao, O.; Yanagida, M.; Himeda, Y.; Sugihara, H.; Kasuga, K. *New J. Chem*. **2006**, *30*, 689. (b) Li, X. H.; Gui, J.; Yang, H.; Wu, W. J.; Li, F. Y.; Tian, H.; Huang, C. H. *Inorg. Chim. Acta* **2008**, *361*, 2835. (c) Fan, S. H.; Wang, K. Z.; Yang, W. C. *Eur. J. Inorg. Chem*. **2009**, 508.

(15) (a) Haga, M. A. *Inorg. Chim. Acta* **1983**, *75*, 29. (b) Ohno, T.; Nozaki, K.; Haga, M. *Inorg. Chem*. **1992**, *31*, 548. (c) Ma, Y. Z.; Yin, H. J.; Wang, K. Z. *J. Phys. Chem. B* **2009**, *113*, 11039. (d) Han, M. J.; Gao, L. H.; Lü, Y. Y.; Wang, K. Z. *J. Phys. Chem. B* **2006**, *110*, 2364. (e) Han, M. J.; Gao, L. H.; Wang, K. Z. *New J. Chem*. **2006**, *30*, 208. (f) Lü, Y. Y.; Gao, L. H.; Han, M. J.; Wang, K. Z. *Eur. J. Inorg. Chem*. **2006**, 430. (g) Bai, G. Y.; Wang, K. Z.; Duan, Z. M.; Gao, L. H. *J. Inorg. Biochem*. **2004**, *98*, 1017. (h) Cao, H.; Ye, B. H.; Li, H.; Li, R. H.; Zhou, J. Y.; Ji, L. N. *Polyhedron* **2000**, *19*, 1975. (i) Cao, H.; Ye, B. H.; Zhang, Q. L.; Ji, L. N. *Inorg. Chem. Commun*. **1999**, *2*, 338.

(16) (a) Sun, M.; Xin, H.; Wang, K. Z.; Zhang, Y. A.; Jin, L. P.; Huang, C. H. *Chem. Commun*. **2003**, 702. (b) Xin, H.; Li, F. Y.; Guan, M.; Huang, C. H.; Sun, M.; Wang, K. Z.; Zhang, Y. A.; Jin, L. P. *J. Appl. Phys*. **2003**, *94*, 4729. (c) Sun, M.; Xin, H.; Zhang, Y. A.; Wang, K. Z.; Jin, L. P.; Huang, C. H. *Huaxue Xuebao* (in Chinese) **2003**, *61*, 1323.(d) Liu, F. R.; Wang, K. Z.; Bai, G. Y.; Zhang, Y. A.; Gao, L. H. *Inorg. Chem*. **2004**, *43*, 1799. (e) Lü, Y. Y.; Gao, L. H.; Han, M. J.; Wang, K. Z. *Eur. J. Inorg. Chem*. **2006**, *430*, 430.

Scheme 1. The Synthetic Routes to **Ru(Hipdpa)** and **Ru(Hpip)**

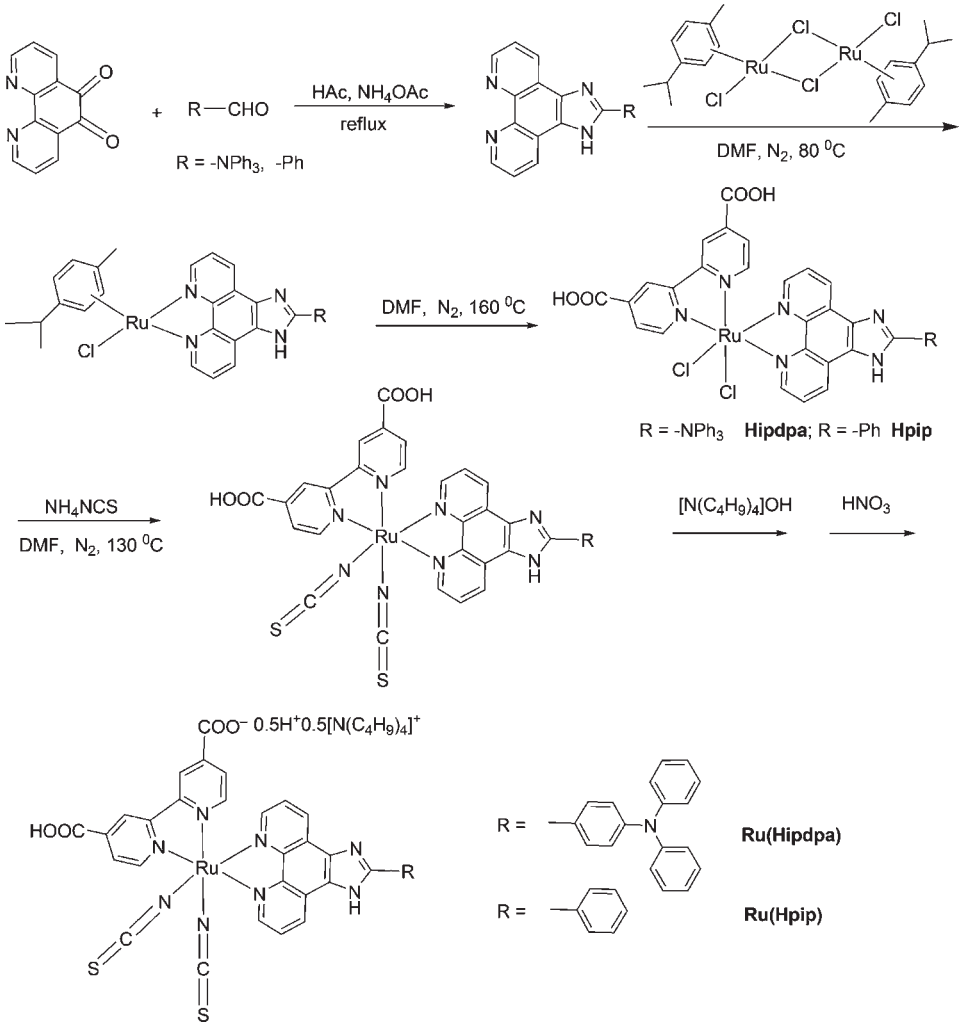

the column. Then the solid was dissolved in basic methanol (tetrabutylammonium hydroxide) solution and purified by passing through a Sephadex LH-20 column with methanol as an eluent. The main red band was collected, and the solvent was evaporated. The resultant solid was dissolved in water, and a few drops of 0.02 M HNO_3 were added to precipitate the product. The mixture was left to stand in a refrigerator overnight. The resulting precipitation was filtered and washed thoroughly with distilled water and vacuo dried, affording the target product in a 30% yield. ^{1}H NMR (400 MHz, DMSO-d_6, δ): 9.53 (d, d, J = 5.08 Hz, 2H), 9.09 (s, 1H), 9.18 (d, J = 8.78 Hz, 1H), 8.90 (s, 1H), 8.45 (d, J = 5.68 Hz, 1H), 8.82 (d, J = 8.86 Hz, 1H), 8.32 (d, J = 5.80 Hz, 1H), 8.20 (d, J = 8.68 Hz, 2H), 7.82 (d, J = 6.23 Hz, 1H), 7.63 (d, J = 5.80 Hz, 2H), 7.44 (d, J = 6.60 Hz, 1H), 7.14−7.41 (m, 12H), 3.06 (t, J = 8.48 Hz, 4H), 1.53−1.60 (m, 4H), 1.26−1.34 (m, 4H), 0.93 (t, J = 7.30 Hz, 6H). IR (KBr): ν = 2959 (w), 2926 (w), 2873 (w), 2102 (vs, $\nu_{C=N}$), 1717 (m, $\nu_{C=O}$), 1592 (vs), 1476 (vs), 1456 (m), 1364 (m), 1317 (m), 1262 (m), 1232 (m, ν_{C-O}), 1193 (m), 1026 (m), 807 (m, $\nu_{C=S}$). MALDI-TOF MS in $(CH_3)_2SO$ (m/z): $[M\text{-}0.5NBu_4^+\text{-}SCN^- + 0.5H^+]^+$ calcd for $RuC_{44}H_{29}N_8O_4S$, 866.90 (100%), found, 867.14; $[M\text{-}0.5NBu_4^+ + 1.5H^+]^+$ calcd for $RuC_{45}H_{30}N_9O_4S_2$, 925.98, found, 926.13 (25%). Anal. calcd for $C_{45}H_{28.5}N_9O_4RuS_2\cdot 0.5N(C_4H_9)_4\cdot DMF\cdot 2H_2O$: C 58.27, H 4.98, N 12.74; Found: C 58.34, H 5.44, N 12.40.

A TPA-free parent complex $[Ru(Hpip)(Hdcbpy)(NCS)_2]^-\cdot 0.5H^+\cdot 0.5[N(C_4H_9)_4]^+$ **Ru(Hpip)** {Hpip = 2-phenyl-1*H*-imidazo-[4,5-*f*][1,10]phenanthroline} was synthesized similarly as a control complex for comparison purposes. The other experimental details are shown in the Supporting Information.

Results and Discussion

Synthesis. Ru(Hipdpa) was synthesized in a one-pot reaction[7a,14,17] with synthetic routes shown in Scheme 1. First, the reaction of Ru-dimer $[RuCl_2(p\text{-cymene})]_2$ with **Hipdpa** according to a 1:2 stoichiometry in DMF at 80 °C resulted in the mononuclear Ru(II) complex. Then H_2dcbpy was added, and the resulting mixture was refluxed for 4 h in DMF at 160 °C under dark. In this process, the cymene ligand from the Ru(II) coordination sphere was replaced by H_2dcbpy. Finally, 20-fold excessive ammonium thiocyanate was added to afford the final product of **Ru(Hipdpa)**. The crude product was purified by a Sephadex LH-20 column with a basic methanol solution of tetrabutylammonium hydroxide as an eluant to remove such side products as S-bonded isomers.[17] The peaks at 0.91−3.14 ppm in the ^{1}H NMR spectrum and the absorption peaks over 2873−2960 cm^{-1} in the FTIR spectrum for **Ru(Hipdpa)**, suggest the presence

(17) Nazeeruddin, M. K.; Zakeeruddin, S. M.; Lagref, J. J.; Liska, P.; Comte, P.; Barolo, C.; VJscardi, G.; Schenk, K.; Grätzel, M. *Coord. Chem. Rev.* **2004**, *248*, 1317.

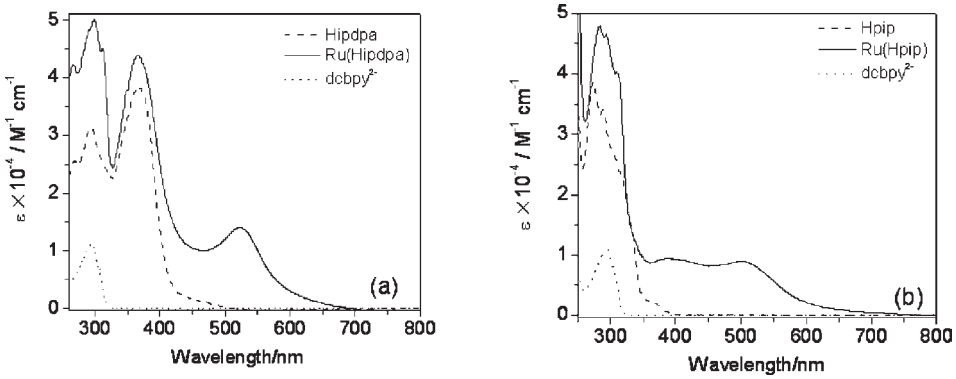

Figure 1. The comparisons of UV−visible spectra of (a) **Ru**(**Hipdpa**) and (b) **Ru**(**Hpip**) with their respective ligands in ethanol solutions.

Table 1. Optical and Electrochemical Data of Ru(II) Complexes and Ligands

	absorption λ_{max}/nm[a] (ε/10^4 M^{-1} cm^{-1})			emission[b]	$E_{1/2}^{ox}$/V[e]	$E_{1/2}^{red}$/V[e]	E_{HOMO}
compound	$\pi \rightarrow \pi^*$ (HL)	$\pi \rightarrow \pi^*$ (dcbpy)	MLCT	λ_{max}/nm (Φ)	$Ru^{III/II}$ Hipdpa dcbpy	HL	E_{LUMO}/eV[f]
Hipdpa	293 (3.15) 365 (3.86)			533 (0.0068)	+0.92	−2.48	
Hpip	274 (3.86) 288 (3.41)			427 (0.188)		−2.29	
$dcbpy^{2-}$[a]		280 (3.12)					
Ru(**Hipdpa**)	300 (4.94) 366 (4.39)	312 (4.58)	525 (1.41)	780 (0.00004)[c]	+0.76 +1.00	−2.14 −1.77	−4.90 −3.15
Ru(**Hpip**)	284 (4.78) 294 (4.65)	310 (4.03) 388 (0.94)	503 (0.90)	644 (0.0012)[d]	+0.77 1.82	−2.20 −	−4.93 −3.16
N3[17]		314 (4.82) 398 (1.40)	539 (1.42)	797 (0.0004)	+0.85	−1.90	−5.15 −3.47[35]

[a] The data were measured in ethanol. [b] Emission data were obtained at room temperature in ethanol. [c] Emission data were obtained at room temperature in ethanol by exciting into the lowest-energy MLCT. [d] Emission data were obtained at room temperature in ethanol by exciting at 467 nm without degassing. [e] The electrochemical data were measured in DMF containing 0.1 M tetrabutyl ammouium hexafluorophosphate using a Pt disk electrode as a working electrode and were reported vs SCE. [f] The energy levels of the highest occupied molecular orbital (HOMO) and the lowest unoccupied molecular orbital (LUMO) were calculated by the following equations: $E_{HOMO} = -4.40 - E_{onset}(ox)$, $E_{LUMO} = E_{HOMO} + E_g$, $E_{onset}(ox)$ is the onset oxidation potential, E_g is the 0−0 transition energy in eV estimated from the onset absorption λ_{onset} (nm) of the dyes, and $E_g = 1240/\lambda_{onset}$ (nm).

of $-C_4H_9$ in both complexes. The NMR spectrum revealed the presence of half of $[N(C_4H_9)_4]^+$ in **Ru**(**Hipdpa**), which is consistent with the elemental analysis result and is also similar to an analoguous complex containing dipyrido[3,2-*a*:2′,3′-*c*]-phenazine reported by Kitao and Kasuga.[14a] We failed in separating the bicarboxylic acid form of **Ru**(**Hipdpa**) even at pH < 1.0, due to the fact that the imidazaole group on **Hipdpa** and **Hpip** protonated at pH < 3.

Absorption and Emission Spectra. Comparisons of UV−visible absorption spectra of **Ru**(**Hipdpa**) and **Ru**(**Hpip**) with their respective ligands are shown in Figure 1, and corresponding absorption spectroscopic data are summarized in Table 1. As shown in Figure 1a, the absorption spectrum of **Ru**(**Hipdpa**) exhibits an intense Hdcbpy-based $\pi-\pi^*$ absorption band at 300 nm ($\varepsilon = 4.94 \times 10^4$ M^{-1} cm^{-1}) with two shoulder peaks being at its higher- and lower-energy sides, respectively, a Hipdpa-based $\pi-\pi^*$ absorption band at 366 nm ($\varepsilon = 4.39 \times 10^4$ M^{-1} cm^{-1}), and a broad metal-to-ligand charger-transfer (^{1}MLCT)[18,19] band at 525 nm ($\varepsilon = 1.41 \times 10^4$ M^{-1} cm^{-1}), which is obviously blue shifted by 14 nm compared to that of **N3**.[17] The above-mentioned $\pi-\pi^*$ absorption band for **Ru**(**Hipdpa**) is different from ligand-based $\pi-\pi^*$ transition bands at 284 ($\varepsilon = 4.78 \times 10^4$), 294 ($\varepsilon = 4.65 \times 10^4$), 310 ($\varepsilon = 4.03 \times 10^4$), and 388 nm ($\varepsilon = 0.94 \times 10^4$ M^{-1} cm^{-1}) for **Ru**(**Hpip**). It is worth mentioning that the MLCT band for **Ru**(**Hipdpa**) is blue shifted by 22 nm and intensified as compared to that of a MLCT band at 503 nm ($\varepsilon = 0.90 \times 10^4$ M^{-1} cm^{-1}) for **Ru**(**Hpip**), due to the stronger electron-donating ability of TPA group on Hipdpa.

The normalized absorption spectra of **Ru**(**Hipdpa**) and **Ru**(**Hpip**) on TiO_2 films and in ethanol are shown in the Supporting Information, Figure S1. **Ru**(**Hipdpa**) and **Ru**(**Hpip**) on TiO_2 exhibit a 25 and 15 nm blue-shifted absorption band compared to their ethanol solutions, respectively, indicating an appreciable interaction between **Ru**(**Hipdpa**) and TiO_2 surface. The ruthenium sensitizers were reported to experience bathochromic or hypsochromic shifts in MLCT bands in the visible region when adsorbed onto TiO_2 surface, such as a hypsochromic shift of 21 nm and a slight blue shift reported for $[Ru(pyrrld_2bpy)_2(H_2dcbpy)]^{2+}$ {pyrrld$_2$bpy = 4,4′-di(pyrrolidin-1-yl)-2,2′-bipyridine}[20a] and **N3**,[20b] respectively, while conversely bathochromic shifts reported for **N719** and $[Ru(H_2dcbpy)_2(bpy\text{-}TPA_2)](PF_6)_2$ {bpy-TPA$_2$ = 4,4′-[([2,2′-bipyridine]-4,4′-diyl)di-(1*E*)-2,1-ethenediyl]bis[*N*,*N*-diphenylbenzenamine]}.[33b]

The emission data of **Ru**(**Hipdpa**) and **Ru**(**Hpip**) are also given in Table 1. **Ru**(**Hipdpa**) is weakly emissive in an air-saturated ethanol solution at room temperature with an emission maximum at 780 nm (λ_{ex} = 525 nm) and a quantum yield of ϕ = 0.00004. However, **Ru**(**Hpip**) in

(18) Juris, A.; Balzani, V.; Barigelletti, F.; Campagna, S.; Belser, P.; von Zelewsky, A. *Coord. Chem. Rev.* **1988**, *84*, 85.
(19) Islam, A.; Sugihara, H.; Arakawa, H. *J. Photochem. Photobiol., A* **2003**, *158*, 131.
(20) (a) Martineau, D.; Beley, M.; Gros, P. C.; Cazzanti, S.; Caramori, S.; Bignozzi, C. A. *Inorg. Chem.* **2007**, *46*, 2272. (b) Shoute, L. C. T.; Loppnow, G. R. *J. Am. Chem. Soc.* **2003**, *125*, 15636.

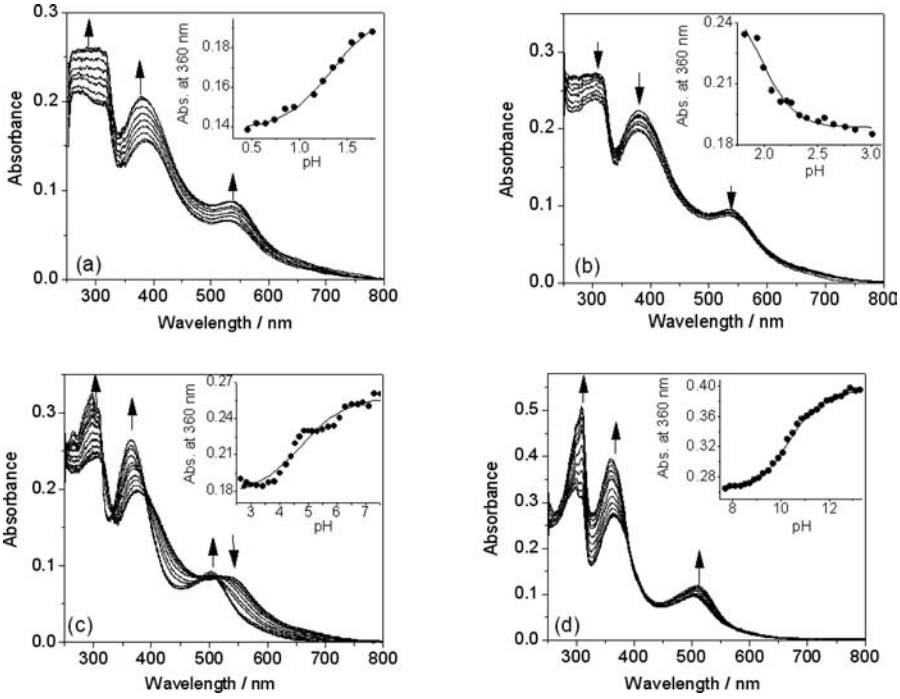

Figure 2. Changes of UV−vis absorption spectra of **Ru(Hipdpa)** upon raising the pH: (a) from 0.45 to 1.77, (b) from 1.82 to 3.00, (c) from 3.50 to 6.50, and (d) from 8.00 to 13.30.

Table 2. The Comparison of Ground- and Excited-State Acidity Ionization Constants for **Ru(Hipdpa)** with Those Reported for Representative Related Ru(II) Complexes

complexes	pK_{ai}	pK_{ai}*	ref
$[Ru(H_2dcbpy)(bpy)_2]^{2+}$	< 0.5, 2.7	3.4, 4.5	21
$[Ru(H_2dcbpy)(dmbip)(CN)]$		2.5, 4.5	23
$[Ru(H_2dcbpy)(dmbip)(H_2O)]$	1.4, 2.2, 11.4		23
$[Ru(H_2dcbpy)(bpy)_2]^{2+}$	1.75, 2.85	4.25	22
$[(bpy)_2Ru(ebipcH_2)Ru(bpy)_2]^{4+}$	4.16, 5.07, 9.65, 12.09	4.54, 5.07, 9.76, 12.09	16d
Ru(Hecip)	< 2.00, 2.67, 4.61, 5.82, 11.58[a]	−, −, −, 7.83, 11.19	24
Ru(Hecip)	0.79, 2.44, 4.29, 6.02, 10.63[b]	−, −, −, 8.09, 9.47	14c
Ru(Hipdpa)	1.33, 1.98, 4.73, 10.36[b]	−, −, 6.78, 9.59	this work
Ru(Hpip)	0.31, 1.24, 4.04, 9.83[b]	−, 0.52, 5.51, 9.18	this work

[a] Aqueous Britton-Robinson buffer solution. [b] Britton-Robinson/DMF (4:1, v/v) buffer; H_2dcbpy = 4,4′-dicarboxylic acid-2,2′-bipyridine; dmbip = 2,6-bis(1-methylbenzimidazol-2-yl)pyridine; ebipcH_2 = *N*-ethyl-4,7-bis([1,10]-phenanthroline[5,6-*f*]imidazol-2-yl)carbazole; eciph = 2-(9-ethyl-9*H*-carbazol-3-yl)-1*H*-imidazo[4,5-*f*][1,10]phenanthroline; and Hecip = 2-(9-ethyl-9*H*-carbazol-3-yl)-1*H*-imidazo[4,5-*f*][1,10]phenanthroline.

ethanol displays a much stronger emission peak at 644 nm with an emission quantum yield of 0.0012, 30-fold that for **Ru(Hipdpa)**. The strongly quenched MLCT excited state of **Ru(Hipdpa)** is probably due to the photoinduced electron-transfer reaction from the TPA group to the excited Ru(III) center.

pH Effects on UV−Vis and Emission Spectra. The UV−vis absorption spectra for **Ru(Hipdpa)** in DMF/Britton-Robinson (BR) buffer (1:4, v/v) as a function of pH are shown in Figure 2. It is clear from Figure 2 that the complex underwent four successive deprotonation processes over a pH range of 0.45−13.00. Upon increasing the pH from 0.45 to 1.77, the absorbance for the MLCT band at 535 nm and the $\pi-\pi^*$ transitions at 290 and 386 nm significantly increased along with a 6 nm blue shift for the later band. The spectral changes observed above are ascribed to the dissociation of the first proton of H_2dcbpy on $[Ru(Hipdpa)(H_2dcbpy)(NCS)_2]$. In contrast, increases in pH from 1.82 to 3.00 resulted in the decreases in the intensities of the bands at 310, 380, and 535 nm, which is assigned to deprotonation of Hdcbpy on $[Ru(Hipdpa)(Hdcbpy)(NCS)_2]^-$. The third deprotonation step observed upon increasing pH from 3.50 to 6.50, and is assigned to the dissociation of one proton on the protonated imidazole ring, resulted in the following spectral changes: the absorption intensities at 310 and 380 nm were obviously increased and blue shifted to 300 and 367 nm, respectively, and the MLCT band was blue shifted from 535 to 502 nm, with the appearance of an isosbestic point at 393 nm. Upon further increasing the pH from 8.00 to 13.30, the last deprotonation of the neutral imidazole ring occurred and was characterized by the evident enhancement in the intensities for the bands at 300 and 360 nm. Quantitative analysis of the absorption changes at 360 nm does show four deprotonation processes, as shown by nonlinear sigmoidal fits of the data in the inset of Figure 2. So, four ground-state ionization constants of $pK_{a1} = 1.33 \pm 0.05$, $pK_{a2} = 1.98 \pm 0.10$, $pK_{a3} = 4.73 \pm 0.14$, and $pK_{a4} = 10.36 \pm 0.04$ were obtained. The pK_{a1} and pK_{a2} values for the deprotonation processes of the two protons on H_2dcbpy with those reported for analogue Ru^{II} complexes are compared in Table 2 and seem reasonable as compared to $pK_{a1} < 0.5$ and $pK_{a2} = 2.7$ reported by Shimidzu et al., $pK_{a1} = 1.75$

Scheme 2. The Ground-State Acid−base Reactions of **Ru**(**Hipdpa**) in a Britton-Robinson/DMF (v/v, 4:1) Buffer Solution

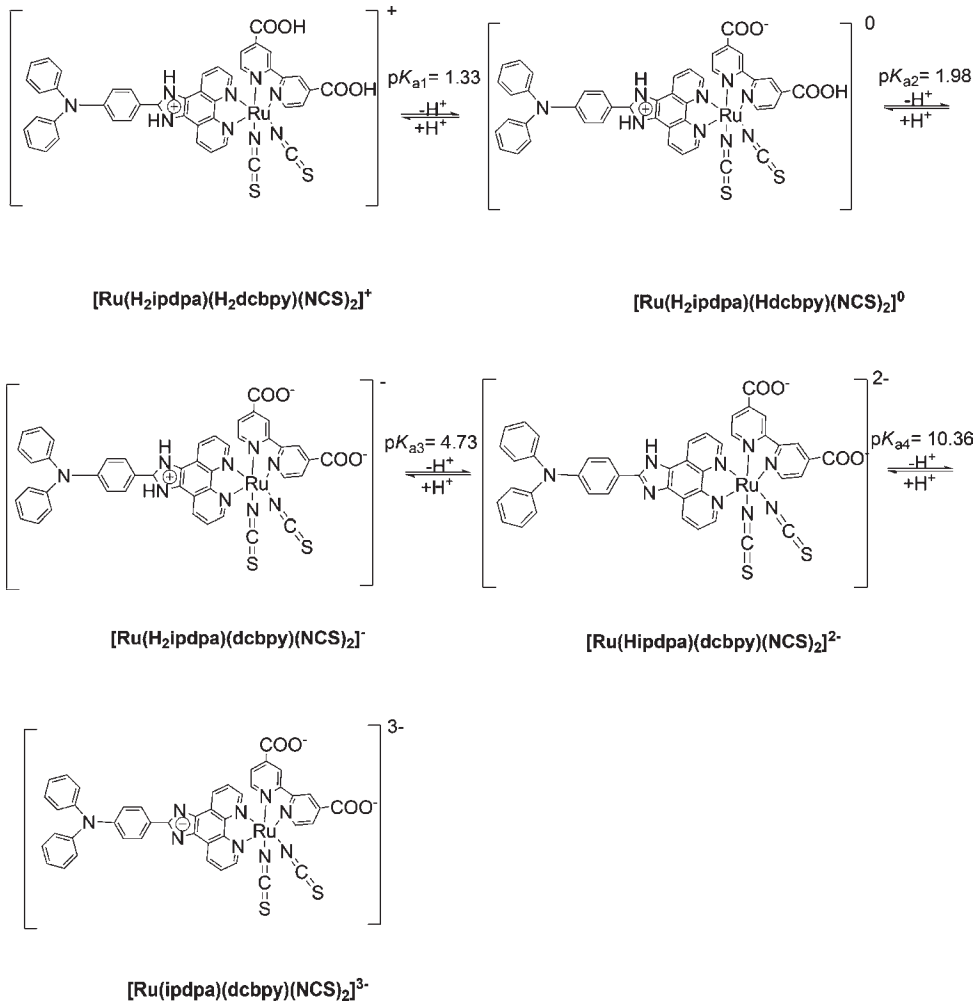

and pK_{a2} = 2.85 reported by Nazeeruddin's group for Ru(dcbpy)(bpy)$_2$,[21,22] and pK_{a1} = 1.4 and pK_{a2} = 2.2 reported for dcbpy ligand on [Ru(dmbip)(dcbpy)(H_2O)] {dmbip = 2,6-bis(1-methylbenzimidazol-2-yl)pyridine} by the Grätzel group[23] as well as pK_{a1} = 0.79 and pK_{a2} = 2.44 we reported for [Ru(Hecip)(Hdcbpy)(NCS)$_2$]$^-$ {Hecip = 2-(9-ethyl-9*H*-carbazol-3-yl)-1*H*-imidazo[4,5-*f*][1,10]phenanthroline}.[14c] A pK_{a3} = 4.73 value observed for the proton dissociation of the protonated imidazole moiety of Hipdpa on the complex is reasonable, as compared to a pK_a value of 4.16 we previously reported for a similar proton dissociation of H_2ebipc on [(bpy)$_2$Ru(H_2ebipc)-Ru(bpy)$_2$]$^{4+}$ {H_2ebipc = *N*-ethyl-4,7-bis([1,10]-phenanthroline[5,6-*f*]imidazol-2-yl)carbazole}[16d] and a pK_a value of 4.29 we recently reported for [Ru(Hecip)(Hdcbpy)-(NCS)$_2$]$^-$.[14c] A pK_{a4} = 10.36 value derived for proton dissociation of the neutral imidazole ring of Hipdpa on the complex is only 0.27 pK_a units less than a pK_a value of 10.63 reported for [Ru(Hecip)(Hdcbpy)(NCS)$_2$]$^-$[14c] but more than 1 pK_a unit than those we reported for a corresponding proton dissociation of a series of Ru(II) complexes with the composition [Ru(bpy)$_2$(N−N)] (N−N = bidentate *N*-heterocyclic ligands),[15c−e] probably due to the presence of two electron-drawing carboxylic groups on [Ru(Hipdpa)(dcbpy)(NCS)$_2$]. On the basis of the above analyses, we summarize protonation/deprotonation processes of **Ru**(**Hipdpa**) in DMF-BR buffer (1:4, v/v) in Scheme 2.

The pH effects on the emission spectra of **Ru**(**Hipdpa**) are shown in Figure 3. Upon raising pH from 4.0 to 8.0, the emission band was blue shifted from 785 to 730 nm with significant increases in emission intensities (Figure 3a). Since this pH range coincides with that observed for the ground-state deprotonation reaction of the protonated imidazole moiety of Hipdpa on the complex in the UV−vis spectrophotometric titration, the above emission spectral changes are thus assigned to the excited-state deprotonation reaction of the same proton, as in the ground state. As shown in the inset of Figure 3a, the complex acted as an "off−on" emission switch with an emission enhancement factor of ~4.7 over the pH region studied. On the contrary, the emission intensities were found to decrease by 43.5% as the pH increased from 8.0 to 12.0 with the emission maxima red shifted from 730 to 750 nm, obviously due to the excited-state deprotonation reaction of the imidazole ring

(21) Shimidzu, T.; Iyoda, T.; Izaki, K. *J. Phys. Chem.* **1985**, *89*, 642.
(22) Nazeeruddin, Md. K.; Kalyanasundaram, K. *Inorg. Chem.* **1989**, *28*, 4251.
(23) Nazeeruddin, M. K.; Müller, E.; Humphry-Baker, R.; Vlachopoulos, N.; Grätzel, M. *J. Chem. Soc., Dalton Trans.* **1997**, 4571.
(24) Fan, S. H.; Yang, W. C.; Wang, K. Z. *Acta Chimica Sinica* (*Huaxue Xuebao*) **2008**, *66*, 690.

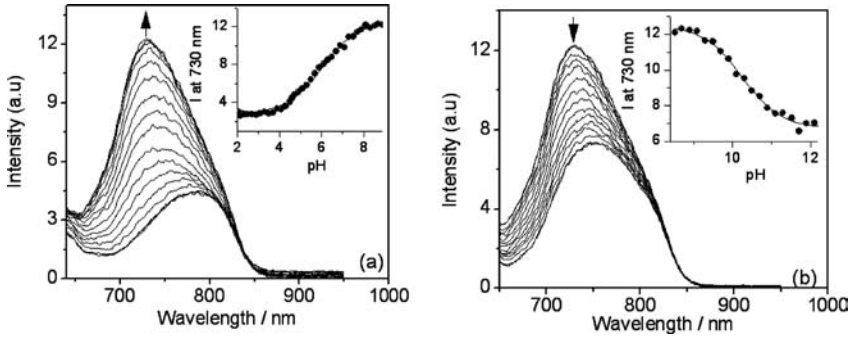

Figure 3. Changes of emission spectra (λ_{ex} = 525 nm) of **Ru**(**Hipdpa**) upon raising the pH: (a) from 4.00 to 8.00 and (b) from 8.00 to 12.00.

on the complex. The emission intensities at 730 nm vs pH profiles (the insets of Figure 3a and b) of the complex were composed of two reverse profiles corresponding to two independent excited-state protonation/deprotonation processes over the pH region from 4.0 to 12.0, namely, a luminescence off−on−off switching action was achieved by the two deprotonation processes of the protonated imidazole moieties on the complex. The pH responsive on−off or off−on luminescence switches are not only fundamental molecular switches but also could be used to mimic many of life processes, such as the functions and activities of "switch on" or "switch off" enzymes within a narrow pH window.[25a−c]

Excited-state ionization constants, pK_a*, could be roughly evaluated on the basis of the Förster cycle,[26] which correlates pK_a* with pK_a thermodynamically by eq 1, where T is temperature (298 K) and ν_B and ν_{HB} denote wavenumber (cm^{-1}) of the deprotonated and the protonated forms, respectively. In practice, ν_B and ν_{HB} are often difficult or even impossible to obtain.

$$pK_a^* = pK_a + (0.625/T)(\nu_B - \nu_{HB}) \quad (1)$$

A good approximation is to use the emission maxima for ν_B and ν_{HB} since the protonation equilibrium is almost certainly established between the ^{3}MLCT states.[27] Therefore, two pK_a* values of pK_{a3}* = 6.78 and pK_{a4}* = 9.59 were obtained. The excited-state pK_{a3}* is 2 pK_a units greater than the ground-state pK_{a3}, indicating that the excited-state electron in $[Ru(H_2ipdpa)(dcbpy)(NCS)_2]^{-*}$ was mostly delocalized over H_2ipdpa rather than dcbpy. The enhanced electron density on H_2ipdpa in the excited $[Ru(H_2ipdpa)(dcbpy)(NCS)_2]^{-*}$ resulted in the greater excited-state pK_{a3}* with respect to the ground-state pK_{a3}, since the acid−base reaction of pK_{a3}* is associated with the proton dissociation of H_2ipdpa^+ in $[Ru(H_2ipdpa)(dcbpy)(NCS)_2]^{-*}$. However, p$K_{a4}$* value is 0.77 p$K_a$ units less than the pK_{a4} value, showing that the electron in the excited-state of $[Ru(Hipdpa)(dcbpy)(NCS)_2]^{2-*}$ was mainly populated on dcbpy rather than Hipdpa, similarly to $[Ru(dmbip)(dcbpy)(CN)]$[23] in which the excited-state electron was evidenced to locate on dcbpy rather than dmbip. Under the same experimental condition, four pK_a values for electron-donating TPA-free $[Ru(H_2pip)(H_2dcbpy)(NCS)_2]^+$ were derived to be 0.31, 1.24, 4.04, and 9.83, which are reasonably less than those found for $[Ru(H_2ipdpa)(H_2dcbpy)(NCS)_2]^+$.

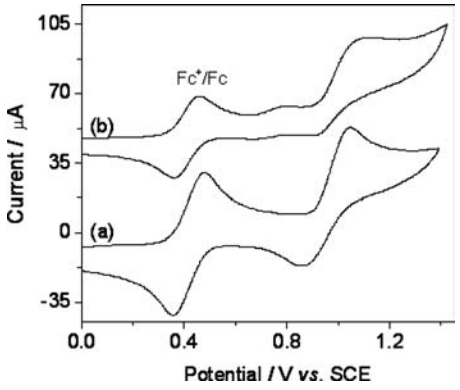

Figure 4. Cyclic voltammograms of (a) **Hipdpa** and (b) **Ru**(**Hipdpa**) in DMF (1.30 mM) recorded at a scan rate of 500 mV/s.

Cyclic Voltammograms. Cyclic voltammograms of **Ru**(**Hipdpa**) and **Ru**(**Hpip**) are compared in Figure 4. **Ru**(**Hipdpa**) in DMF revealed a quasi-reversible oxidative process $E_{1/2}$ = +0.76 V and a quasi-reversible oxidative process at $E_{1/2}$ = +1.00 V. The former oxidation is assigned to a $Ru^{III/II}$ couple with the $E_{1/2}$ value being almost as same as the $E_{1/2}$ value of +0.78 V found for **Ru**(**Hpip**) and is also in good agreement with $E_{1/2}$ = +0.73 ∼ +0.78 V reported for $Ru(H_2dcbpy)(dmbpy)(NCS)_2$ (dmbpy = 4,4′-dimetyl-2,2′-bipyridine),[17] which is shifted negatively by 0.09 V compared to the **N3** couple,[17] indicating stronger electron-donating ability of Hipdpa than H_2dcbpy. The latter oxidation for **Ru**(**Hipdpa**) is assigned to a TPA-based $Hipdpa^{I/0}$ redox couple as comparison with an almost same $E_{1/2}$ value of +0.92 V found for free Hipdpa (Figure 4a), indicating that different electron-transfer reactions occurred on the Ru(II) and TPA moieties.[12b,28] At negative potentials, **Ru**(**Hipdpa**) in DMF exhibited a reversible redox couple at $E_{1/2}$ = −1.77 and a quasi-reversible one at $E_{1/2}$ = −2.14 V vs SCE, which are assigned to the reduction of Hdcbpy and the imidazo[4,5-*f*][1,10]phenanthroline moiety on Hipdpa, respectively, and are 50 and 60 mV more positive than the two redox couples found at −1.82 and −2.20 V for **Ru**(**Hpip**), respectively. For the metal- and ligand-based redox processes, the voltammetric peak

(25) (a) Gunnlaugsson, T.; Leonard, J. P.; Snchal, K.; Harte, A. J. *J. Am. Chem. Soc.* **2003**, *125*, 12062. (b) Pallavicini, P.; Amendola, V.; Massera, C.; Mundum, E.; Taglietti, A. *Chem. Commun.* **2002**, 2452. (c) Fabbrizzi, L.; Gatti, F.; Pallavicini, P.; Parodi, L. *New J. Chem.* **1998**, *22*, 1403.

(26) Donckt, E. V. *In progress in Reaction Kinetic*, 5th ed.; Poter, G., Ed.; Pergamon Press: Oxiford, England, 1970.

(27) Zheng, G. Y.; Wang, Y.; Rillema, D. P. *Inorg. Chem.* **1996**, *35*, 7118.

(28) Bignozzi, C. A.; Argazzi, R.; Kleverlaan, C. J. *Chem. Soc. Rev.* **2000**, *29*, 87.

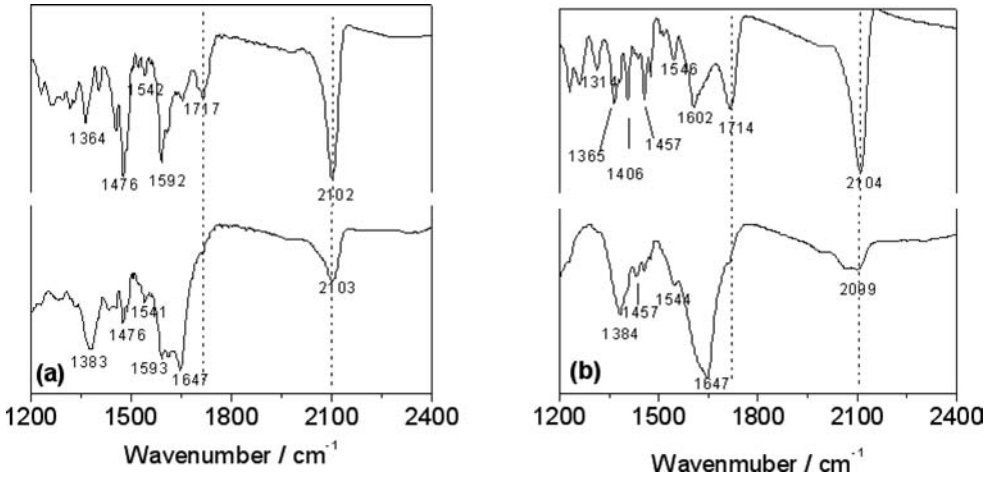

Figure 5. FTIR spectra of (a) **Ru(Hipdpa)** and (b) **Ru(Hpip)** in a KBr pellet (top) and in absorbed film on TiO_2 (bottom).

currents are proportional to the square root of the scan rates, showing diffusion-controlled redox processes. The excited-state oxidation potential of a sensitizer, $E^*(Ru^{III/II})$, which plays an important role in the electron-transfer process, can be approximately calculated from the ground-state potential $E(Ru^{III/II})$ and the 0−0 excitation energy (E_{0-0}), according to the equation[29] $E^*(Ru^{III/II}) = E(Ru^{III/II}) - E_{0-0}$. The $E^*(Ru^{III/II})$ values of **Ru(Hipdpa)** and **Ru(Hpip)** are derived to be −0.99 and −1.00 V vs SCE on the basis of the E_{0-0} values of 1.75 and 1.77 eV, calculated from a visible absorption edge of 710 and 700 nm, and $E_{1/2}$ ($Ru^{III/II}$) values of +0.76 V and +0.77 V vs SCE, respectively, which are sufficiently more negative than the conduction band edge level of the TiO_2 at approximately −0.7 V vs SCE,[1b,30] indicating energically highly favorable for electron injection from the excited dyes into the conduction band of TiO_2. Moreover, the energy levels of the frontier orbitals of dye molecule also have an effect on the electron-transfer processes in DSSCs.[12h,31] So, we estimated the energy levels of the highest occupied molecular orbital (HOMO) and the lowest unoccupied molecular orbital (LUMO) from the onset oxidation potentials and the absorption edge of these dyes (see Table 1). The data indicate that the HOMO energy levels of **Ru(Hipdpa)** and **Ru(Hpip)** are higher than that of **N3** because the oxidation potentials were negatively shifted relative to that of **N3**. Furthermore, the LUMOs for **Ru(Hipdpa)** (−3.15 eV) and **Ru(Hpip)** (−3.16 eV) are higher than the conduction band (CB) energy level of the TiO_2 (−4.0 eV) and guarantee more efficient electron injection into TiO_2 conduction band.

FTIR Spectra. The FTIR spectra of **Ru(Hipdpa)** and **Ru(Hpip)** in KBr pellets and in the absorbed form onto TiO_2 films are shown in Figure 5. An intense N-coordinated $\nu_{C=N}$ absorption band was found to be at 2102 cm^{-1} for **Ru(Hipdpa)** and 2104 cm^{-1} for **Ru(Hpip)**. This band is approximatly 1.6 times more intense than the $\nu_{C=S}$ band at 807 cm^{-1}. A broad and medium-intensity band was found at 1717 cm^{-1} for **Ru(Hipdpa)** and 1714 cm^{-1} for **Ru(Hpip)** due to $\nu_{C=O}$ of carboxy group, which

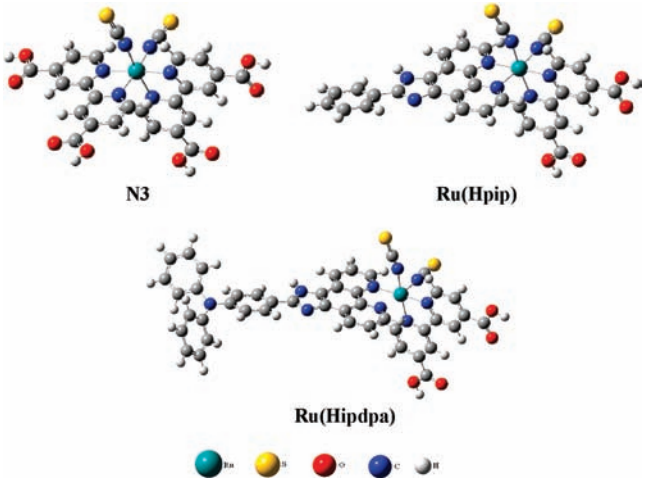

Figure 6. The optimized molecular structures of fully protonated **N3**, **Ru(Hpip)**, and **Ru(Hipdpa)**.

is close to those reported for related ruthenium dyes **K8** and **K9**.[32] The four bands at ∼1592, 1476, 1456, and 1405 cm^{-1} are assigned to the ring-stretching modes of the ligand, and the appearance of the peaks at ∼2959, 2926, and 2873 cm^{-1} indicates the presence of the tetrabutyl ammonium ion.[32b] The FTIR spectra of **Ru(Hipdpa)** and **Ru(Hpip)** anchored onto the TiO_2 film clearly show the absence of above-mentioned $\nu_{C=O}$ of −COOH and the presence of carboxylate asymmetric- and symmetric-stretching vibrations at 1593 and 1383 cm^{-1} for **Ru(Hipdpa)** and 1601 and 1384 cm^{-1} for **Ru(Hpip)**, indicating that the carboxylic group on **Ru(Hipdpa)** and **Ru(Hpip)** has dissociated and was involved in the adsorption onto the TiO_2 surface. The ν_{NCS} signals observed at 2103 and 2099 cm^{-1} for **Ru(Hipdpa)** and **Ru(Hpip)** are close to 2102 and 2104 cm^{-1} observed for **Ru(Hipdpa)** and **Ru(Hpip)** in KBr pellets, respectively, indicating that ν_{NCS} was almost unaffected by the adsorption process.

(29) Caspar, J. V.; Westmoreland, T. D.; Allen, G. H.; Bradley, P. G.; Meyer, T. J.; Woodruff, W. H. *J. Am. Chem. Soc.* **1984**, *106*, 3492.
(30) Liu, G.; Jaegermann, W.; He, J.; Sundstrom, V.; Sun, L. *J. Phys. Chem. B* **2002**, *106*, 5814.
(31) Gratzel, M. *J. Photochem. Photobiol., A* **2004**, *164*, 3.
(32) (a) Renouard, T.; Fallahpour, R. A.; Nazeeruddin, Md. K.; Humphry-Baker, R.; Gorelsky, S. I.; Lever, A. B. P.; Gratzel, M. *Inorg. Chem.* **2002**, *41*, 367. (b) Barolo, C.; Nazeeruddin, Md. K.; Fantacci, S.; Di Censo, D.; Comte, P.; Liska, P.; VJscardi, G.; Quagliotto, P.; De Angelis, F.; Ito, S.; Gratzel, M. *Inorg. Chem.* **2006**, *45*, 4642. (c) Nazeeruddin, Md. K.; Grätzel, M. *J. Photochem. Photobiol., A* **2001**, *145*, 79. (d) Nazeeruddin, Md. K.; Klein, C.; Liska, P.; Grätzel, M. *Coord. Chem. Rev.* **2005**, *249*, 1460.

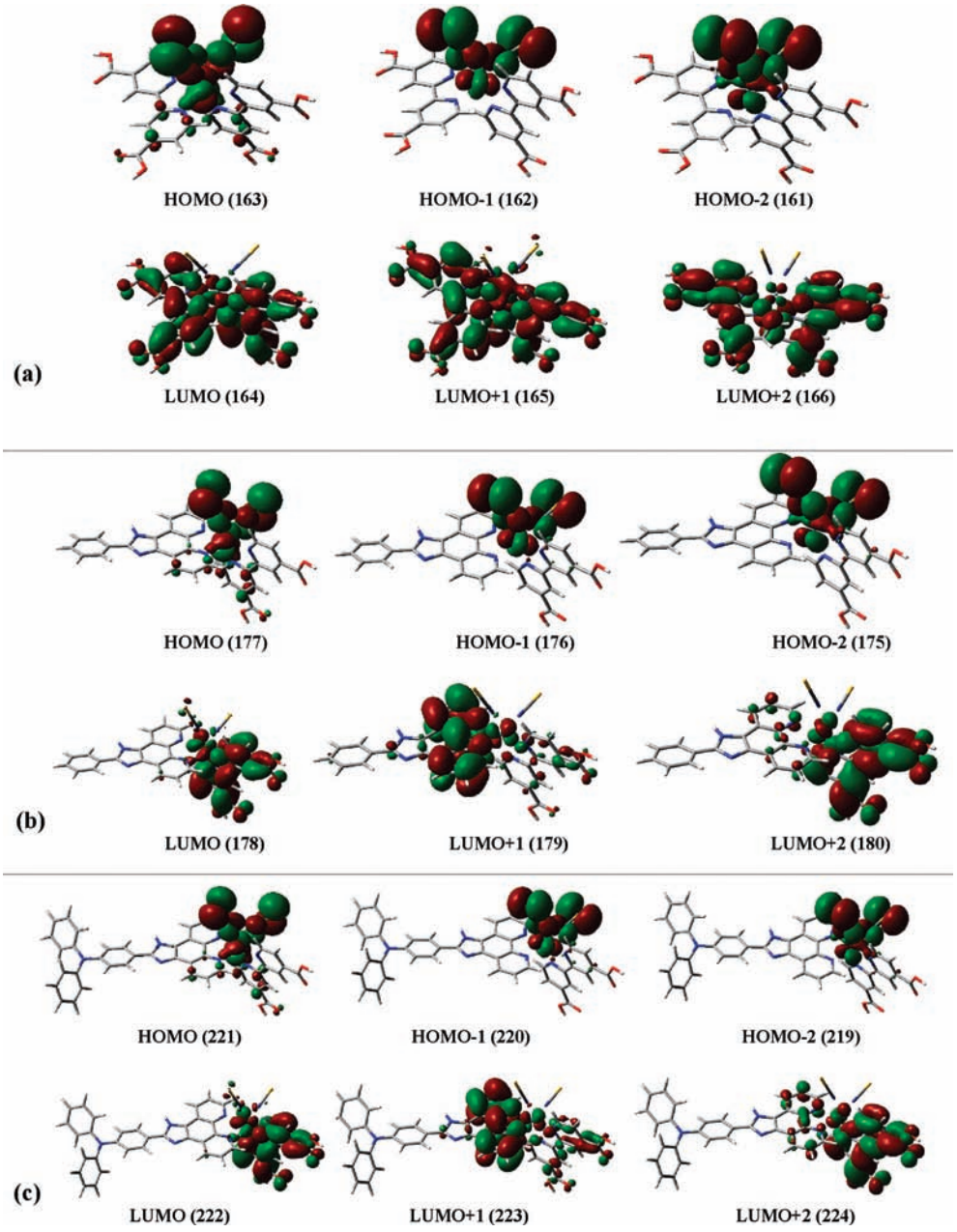

Figure 7. Graphical representations of the frontier orbitals of the fully protonated (a) **N3**,(b) **Ru**(**Hpip**), and (c) **Ru**(**Hipdpa**).

IR spectroscopy is also a powerful tool for the investigation of binding modes of carboxylate of Ru(II) dyes to TiO_2 nanocrystalline films.[7b,d,33−35] The values of frequency difference $\Delta\nu$ ($\Delta\nu = \nu_{asym,COO^-} - \nu_{sym,COO^-}$) between COO^- antisymmetric and symmetric stretches were observed at 228 and 237 $cm^{-1}$for **Ru**(**Hipdpa**) and Ru(Hpip) in KBr pellets {ν_{asym,COO^-} = 1592 cm^{-1} and ν_{sym,COO^-} = 1364 cm^{-1} for **Ru**(**Hipdpa**); ν_{asym,COO^-} = 1602 and ν_{sym,COO^-} = 1365 cm^{-1} for **Ru**(**Hpip**)} are higher than $\Delta\nu$ values of 210 and 217 cm^{-1} found for **Ru**(**Hipdpa**) and **Ru**(**Hpip**) anchored onto TiO_2, respectively, suggesting that the carboxylates groups in Ru(Hipdpa) and **Ru**(**Hpip**) are coordinated via bridging or bidentate mode to the TiO_2 surface rather than an ester-type linkage, similarly to $(Bu_4N)_2[Ru(Hdcbpy)_2(NCS)_2]$ (**N719**)[36b] and other analogous Ru(II) complexes.[7b,d,33a,d−f,34] By using bipyridine $\nu_{C=C}$ at 1542 cm^{-1} as an internal standard, the absorbed film showed an attenuation in the intensity of ν_{C-O} for nonequivalent

(33) (a) Fillinger, A.; Parkinson, B. A. *J. Electrochem. Soc.* **1999**, *146*, 4559. (b) León, C. P.; Kador, L.; Peng, B.; Thelakka, M. *J. Phys. Chem. B* **2006**, *110*, 8723. (c) Murakoshi, K.; Kano, G.; Wada, Y.; Yanagida, S.; Miyazaki, H.; Matsumoto, M.; Murasawa, S. *J. Electroanal. Chem.* **1995**, *396*, 27. (d) Nara, M.; Torii, H.; Tasumi, M. *J. Phys. Chem.* **1996**, *100*, 19812. (e) Shklover, V.; Ovehinnikov, Y. E.; Braginsky, L. S.; Zakeerddin, S. M. M.; Grätzel *Chem. Mater.* **1998**, *10*, 2533. (f) Duffy, N. W.; Dobson, K. D.; Gordon, K. C.; Robinson, B. H.; NcQuillan, A. J. *Chem. Phys. Lett.* **1997**, *266*, 451.
(34) Kong, F. T.; Dai, S. Y.; Wang, K. J. *Chin. J. Chem.* **2007**, *25*, 168.
(35) Finnie, K. S.; Bartlett, J. R.; Woolfrey, J. L. *Langmuir* **1998**, *14*, 2744.
(36) (a) Fantacci, S.; De Angelis, F.; Selloni, A. *J. Am. Chem. Soc.* **2003**, *125*, 4381. (b) Jose, R.; Kumar, A.; Thavasi, V.; Fujihara, K.; Uchida, S.; Ramakrishna, S. *Appl. Phys. Lett.* **2008**, *93*, 023125. (c) De Angelis, F.; Fantacci, S.; Selloni, A. *Chem. Phys. Lett.* **2004**, *389*, 204. (d) Shklover, V.; Ovchinnikov, Y. E.; Braginsky, L. S.; Zakeeruddin, S. M.; Grätzel, M. *Chem. Mater.* **1998**, *10*, 2533.

oxygen at 1234 cm^{-1}, instead a dominant band for equivalent-oxygen $\nu_{as,\ COO^-}$ and $\nu_{s,\ COO^-}$ vibrations as compared to the KBr pellet, also supporting a bridging or bidentate anchoring mode of the Ru(II) complex on the TiO_2 surface.[33b]

Computational Studies. The geometries of the fully protonated complexes were optimized by DFT calculations at the B3LYP/6-31G* and are shown in Figure 6. Partial data of the optimized bond lengths and angles are shown in the Supporting Information, Table S1. The optimized **N3** structure is in good agreement with that reported in the literature.[36] Similarly to **N3**, the orbital profiles for HOMO, HOMO-1, HOMO-2, LUMO, LUMO+1, and LUMO+2 of **N3**, **Ru(Hpip)**, and **Ru(Hipdpa)** are presented in Figure 7. The HOMO, HOMO-1, and HOMO-2 of **Ru(Hpip)** and **Ru(Hipdpa)** have smaller amplitudes on the ruthenium metal t_{2g} character and much larger amplitudes on the thiocyanate (NCS) ligands, more specially are primarily located on the sulfur atom. The most remarkable difference among **N3**, **Ru(Hpip)**, and **Ru(Hipdpa)** can be found in the descriptions of the HOMO-4 in the Supporting Information, Figure S2. The HOMO-4 for **N3** and **Ru(Hpip)** is a combination of Ru t_{2g} and NCS π orbitals, whereas the HOMO-4 of **Ru(Hipdpa)** is only contributed from TPA on Hipdpa. Furthermore, the HOMO-4 energy value in **Ru(Hipdpa)** is 1.10 and 0.76 eV higher than those of **N3** and **Ru(Hpip)**, respectively (Scheme 3). In contrast, the electrons on the LUMO of **Ru(Hpip)** and **Ru(Hipdpa)** can be seen to be more localized over the diimine framework of the H_2dcbpy ligand with appreciable electron density on the oxygen atoms of the carboxyl groups, which indicates that electronic coupling of LUMO with the titanium 3d orbitals that form the conduction band of TiO_2 is indeed present in these dye-sensitized solar cells.[37] These results suggest that **Ru(Hpip)** and **Ru(Hipdpa)** dyes could act as efficient photosensitizers for DSSCs, since two H_2dcbpy ligands on **N3** cannot bind to TiO_2 particles simultaneously and the excited electron on the H_2dcbpy moiety that is not directly connected to TiO_2 provides a very small contribution to the conversion efficiency of the DSSCs. The LUMO+1 of **Ru(Hpip)** and **Ru(Hipdpa)** is mainly localized on the modified phenanthroline ligands of Hpip and Hipdpa, while that of **N3** is contributed from the H_2dcbpy ligand. Such locations of LUMO and LUMO+1 levels have been reported for other ruthenium complexes, in which LUMO and LUMO+1 are localized on the two different ligands.[38] In addition, for a high-efficiency sensitizer, the LUMO energy level should match with the lower limit of the conduction band of TiO_2. As can also be seen from Scheme 3, LUMOs of **Ru(Hipdpa)**, **Ru(Hpip)** and **N3** are located at −2.83, −2.88, and −3.18 eV, respectively, which are higher than the bottom of the conduction band of TiO_2, and therefore, **Ru(Hipdpa)** and **Ru(Hpip)** can be expected to inject excited electrons into the conduction band of TiO_2 more favorably than **N3**. The HOMO−LUMO energy gaps increase by an order of **N3** (1.62 eV) < Ru(Hipdpa) (1.66 eV) < **Ru(Hpip)** (1.67 eV), which is in agreement with the energy order from the viewpoint of absorption edges of **N3**, **Ru(Hpip)**, and **Ru(Hipdpa)**.

Scheme 3. Molecular Orbital Energy Diagrams of Fully Protonated Ru(II) Complexes **N3**, **Ru(Hpip)**, and **Ru(Hipdpa)**[a]

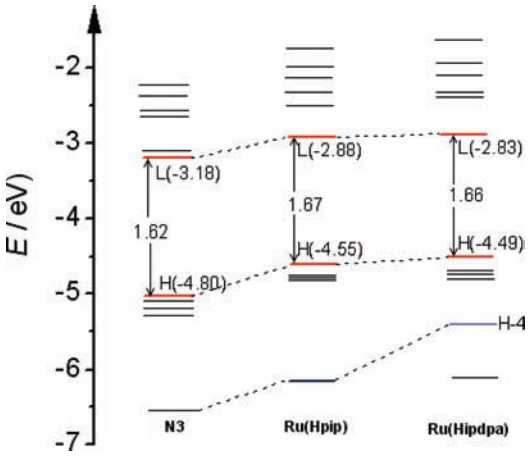

[a] The HOMO−LUMO gaps are reported in eV (DFT/B3LYP/LanL2DZ and 6-31G*).

Photovoltaic Performance. The incident monochromatic photon-to-current conversion efficiency (IPCE) and the overall light-to-electric power conversion efficiency (η) of the solar cells are evaluated according to eqs 2 and 3, respectively.

$$\mathrm{IPCE}(\%) = \frac{1240 \times J_{sc}}{\lambda \times \varphi} \times 100 \qquad (2)$$

$$\eta = \frac{ff \times V_{oc} \times J_{sc}}{\varphi} \qquad (3)$$

Where J_{sc} is the short-circuit photocurrent density (mA cm^{-2}), V_{oc} is the open-circuit voltage (V), *ff* is the fill factor of the cell, ϕ is the incident photon flux (mW cm^{-2}), and λ is the incident light wavelength (nm). As shown in Figure 8, the plots of monochromatic IPCE as a function of excitation wavelength of **Ru(Hipdpa)**, **Ru(Hpip)**, and **N3**-based cells band shapes closely parallel the absorption spectra for the dyes on the TiO_2 films, indicating the photoelectric effects originated from the Ru(II) dyes. The IPCE of **Ru(Hipdpa)**-based DSSC reached its maximum value of 85% at ~520 nm, which is 30% greater than that (55%) of **Ru(Hpip)** and close to that (87%) of **N3**. As shown in Figure 9 and in Table 3, **Ru(Hipdpa)**-based cell showed J_{sc}, V_{oc}, and η up to 18.7 mA cm^{-2}, 630 mV, and 6.85%, respectively, while **Ru(Hpip)**-based cell gave much poorer device parameters with J_{sc}, V_{oc}, and η only to 7.6 mA cm^{-2}, 546 mV, and 2.48%, respectively. Obviously, the significantly improved performance observed for the **Ru(Hipdpa)**-based cell compared to the **Ru(Hpip)**-based cell is due to the grafting of the TPA group to 2-phenyl-1*H*-imidazo[4,5-*f*][1,10]phenanthroline. The TPA moiety in **Ru(Hipdpa)** acts as an electron-donating group to red shift the maximum absorption wavelength of the MLCT transition and to enhance the molar absorption coefficient with respect to **Ru(Hpip)**, thus increasing

(37) Srikanth, K.; Marathe, V. R.; Mishra, M. K. *Inter. J. Quantum Chem.* **2002**, *89*, 535.
(38) (a) Wang, P.; Klein, C.; Humphry-Baker, R.; Zakeeruddin, S. M.; Grätzel, M. *J. Am. Chem. Soc.* **2005**, *127*, 808. (b) Nazeeruddin, M. K.; Bessho, T.; Cevey, L.; Ito, S.; Klein, C.; De Angelis, F.; Fantacci, S.; Comte, P.; Liska, P.; Imai, H.; Grätzel, M. *J. Photochem. Photobiol., A* **2007**, *185*, 331. (c) Abbotto, A.; Barolo, C.; Bellotto, L.; De Angelis, F.; Grätzel, M.; Manfredi, N.; Marinzi, C.; Fantacci, S. J.; Yum, H.; Nazeerudin, M. D. *Chem. Commun.* **2008**, 5318.

the photocurrent due to the increase in light-harvesting ability. Surprisingly, we found that the overall light-to-electric power conversion efficiency of the **Ru(Hipdpa)**-sensitized cell are close to an efficiency of $\eta = 6.47\%$ observed for **N3**-sensitized cell, even though **Ru(Hipdpa)** was less adsorbed onto TiO_2 surface than **N3**. The quantity of the dyes adsorbed on TiO_2 was estimated by desorbing the complex from the TiO_2 film into a 0.02 M NaOH−methanol (v/v, 1:1) solution and measuring the absorption spectra of the resultant solutions. The amounts of **Ru(Hpip)**, **Ru(Hipdpa)**, and **N3** adsorbed on the TiO_2 electrode were calculated to be 1.51×10^{-7}, 1.12×10^{-7}, and 4.70×10^{-7} mol cm^{-2}, respectively. Importantly, the **Ru(Hipdpa)**-based device even exhibited a 30 mV increase in V_{oc} relative to **N3**. Meyer[12a] and Bonhôte[12g] et al. have attributed the observed increases in open-circuit photovoltages for phenothiazine- (PNT)- or TPA-containing Ru(II) sensitizers to the retardation of electron recombination dynamics through multistep charge-transfer cascades, namely, following the electron transfer from excited Ru(II) chromophores to the conduction band of TiO_2, the TPA or PNT group may reduce the oxidized Ru center to give a positive charge (hole) on the TPA or PNT moiety, making the physical distance between the two charge-separated states of the TPA or PNT moiety and the conduction band of TiO_2 much longer than that of two primary charge-separated states of the TPA or PNT moiety-free Ru center and the conduction band of TiO_2, thus contributing a net effect to extend the lifetime of the charge-separated state.[12a,c,f,g] Recently, the Thelakkat group has successfully applied donor-antenna TPA- and tetraphenylbenzidine-containing ruthenium dyes for solid-state sensitized solar cells with improved device performance in comparison to the **N719** dye because of the combination of an efficient light-harvesting feature and a retardation of electron recombination process.[12b] On the contrary, the TPA in **Ru(Hipdpa)** we studied here could not reduce the oxidized Ru center to give a positive charge (hole) on the TPA, since an $E_{1/2}$ value of 1.00 V vs SCE for (TPA^+/TPA) in **Ru(Hipdpa)** is more positive than an $E_{1/2}$ value of 0.77 V vs SCE for {Ru(III)/Ru(II)} in **Ru(Hipdpa)** (see Table 1). Namely, the regeneration reaction of the sensitizer by the hole transfer from the oxidized ruthenium sensitizer to the TPA moiety, as previously reported for the TPA-containing Ru(II) sensitizers, would not occur in the **Ru(Hipdpa)**-based solar cell we studied. Therefore, it is conceivable that there are unknown factors which made a significant contribution to the enhanced photoelectric performance for the device we studied.

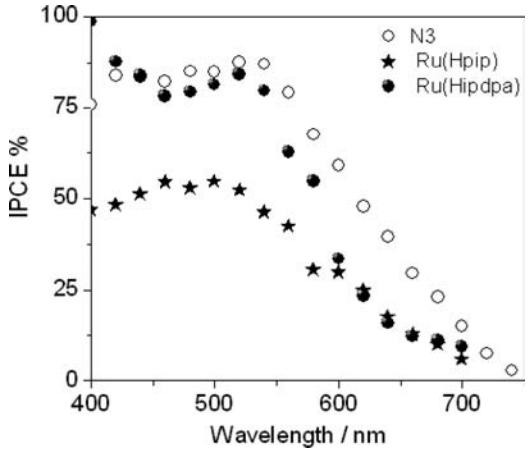

Figure 8. The plots of IPCE values vs excitation wavelengths for **Ru(Hipdpa)**-, **Ru(Hpip)**-, and **N3**-sensitized TiO_2 nanocrystalline solar cells. Mediator: 0.05 M I_2, 0.5 M LiI, and 0.5 M 4-*tert*-butylpyridine in 50% acetonitrile and 50% PC.

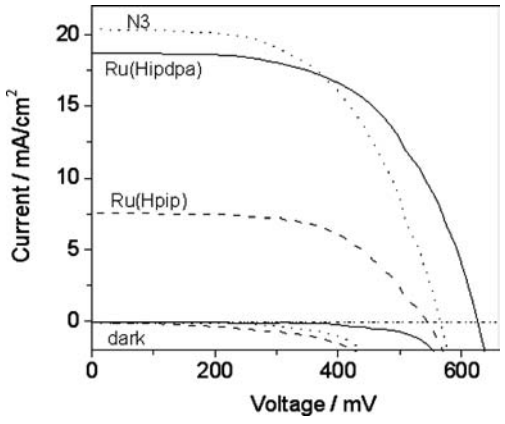

Figure 9. The photocurrent voltage characteristics of **Ru(Hipdpa)**-, **Ru(Hpip)**-, and **N3**-sensitized TiO_2 nanocrystalline solar cells. Mediator: 0.05 M I_2, 0.5 M LiI, and 0.5 M 4-*tert*-butylpyridine in 50% acetonitrile and 50% PC.

Conclusions

Grafting of a TPA group onto TPA-free parent complex **Ru(Hpip)** to give a new complex **Ru(Hipdpa)**, which has a red-shifted metal-to-ligand charge-transfer (MLCT) absorption

Table 3. The Photovoltaic Performance of DSSCs Based on **Ru(Hipdpa)**, **Ru(Hpip)**, and **N3**

dyes[a]	ϕ (mW cm^{-2})	V_{oc} (mV)	J_{sc} (mA cm^{-2})	*ff* (%)	η (%)	IPCE_{max}(%)	ref
Ru(Hipdpa)	100	630	18.7	58.1	6.85	85	this work[b]
Ru(Hpip)	100	546	7.8	60.1	2.48	55	this work[b]
Ru(TPA)		767	4.4	34	1.5	−	12b, 12c
Ru(TPD)		757	9.6	35	3.4	−	12d
Ru(MPPyA)		630	17.9	70	7.9	87	12h
N3	100	600	20.3	56.0	6.47	87	this work
N3		600	19.0	65	7.4	85	4[c]
N3		580	1.26	62	4.54	40	7c[d]
N3		686	11.1	72	5.5	−	34[e]

[a] TPA = 4, 4′-bis(4-diphenylaminostyryl)-2, 2′-bipyridine; TPD = 4,4′-bis(*N*-(phenyl)-*N*′-(styryl)-*N*,*N*′-bis(3-methyl phenyl)-1,1′-biphenyl-4,4′-diamino)-2,2′-bipyridine; and MPPyA = *N*-(4-methoxyphenyl)-*N*-(pyridin-2-yl)pyridin-2-amine. [b] Measured in 0.05 M I_2, 0.5 M LiI, and 0.5 M 4-*tert*-butylpyridine in acetonitrile:PC (1:1,v/v). [c] Measured in 0.5 M tetrabutylammonium iodide, 0.02 M LiI, 0.05 M I_2, and 0.5 M 4-*tert*-butylpyridine that was dissolved in acetonitrile. [d] Measured in 0.6 M 1-propyl-3-methylimidazolium iodide, 0.05 M I_2, 0.05 M LiI, and 0.5 M *tert*-butylpyridine in 3-methoxypropionitrile. [e] 0.05 M I_2, 0.5 M LiI, and 0.5 M *tert*-butylpyridine in acetonitrile/PC (1:1,v/v).

band with an enhanced molar absorptivities relative to **Ru(Hpip)**. The spectrophotometric pH titrations indicated that **Ru(Hipdpa)** exhibited four independent protonation/deprotonation processes in the ground state and two observable protonation/deprotonation processes in the excited state, with one of the protonation/deprotonation processes in both the ground and excited state, occurring near the physiological pH region. **Ru(Hipdpa)** was shown to act as off−on−off-type emission switches when excited at 525 nm. **Ru(Hipdpa)** has been evidenced to covalently bind to a TiO_2 nanocrystalline surface in a bridging or bidentate anchoring mode by IR spectroscopy. The **Ru(Hipdpa)**-sensitized TiO_2 nanocrystalline solar cell exhibited a significantly enhanced open-circuit voltage and short-circuit photocurrent density and an overall light-to-electric power conversion efficiency as compared to the **Ru(Hpip)**-based device, due partially to the enhancement in the light-harvesting ability, but the regeneration reaction of the oxidized ruthenium sensitizer by the hole transfer to the TPA moiety, as previously reported for the TPA-containing Ru(II) sensitizers, could be excluded in the **Ru(Hipdpa)**-based device we studied. A more detailed study on the photoelectric mechanism is in progress.

Acknowledgment. The authors thank the National Natural Science Foundation (20771016, 20971016, 20871011, and 90922004), the Beijing Natural Science Foundation (2072011), the Research Fund for the Doctoral Program of Higher Education (20060027002), and the Analytical and Measurements Fund of Beijing Normal University for financial support.

Supporting Information Available: The detailed description of materials and reagents, analytical measurements, computational methods, preparation of dye-adsorbed TiO_2 films, dye-sensitized solar cell fabrication, photoelectrochemical measurements, a comparison of normalized visible absorption spectra of **Ru(Hipdpa)** and **Ru(Hpip)** adsorbed on TiO_2 film and dissolved in ethanol, and the profiles of the HOMO-4 of **N3**, **Ru(Hpip)**, and **Ru(Hipdpa)**, and the partial data of optimized bond lengths and angles. This material is available free of charge via the Internet at http://pubs.acs.org.